Adaptive-optics corrections available for the whole sky

Roberto Ragazzoni*, Enrico Marchetti† & Gianpaolo Valente‡

** Astronomical Observatory of Padova vicolo dell'Osservatorio 5, I-35122 Padova, Italy*
† Centro Galileo Galilei, Apartado de Correos 565, E-38700 Santa Cruz de la Palma, Spain
‡ Department of Physics and INFN (sez. PD), University of Padova, via F. Marzolo 8, I-35131 Padova, Italy

Adaptive-optics systems can in principle allow a telescope to achieve performance at its theoretical maximum (limited only by diffraction), by correcting in real time for the distortion of starlight by atmospheric turbulence[1]. For such a system installed on an 8-m-class telescope[2,3], the spatial resolution and sensitivity could be up to 100 times better than conventional imaging[4,5]. Adaptive-optics corrections have hitherto been achieved only for regions of the sky within a few arcseconds of a bright reference source. But it has been proposed theoretically that by using multiple guide stars, the tomography of atmospheric turbulence could be probed and used to extend adaptive-optics corrections to the whole sky[6,7]. Here we report the experimental verification of such tomographic[8] corrections, using three off-axis reference stars ~15 arcsec from the central star. We used the observations of the off-axis stars to calculate the deformations of the wavefront of the central star, and then compare them with the real measured values. This tomographic approach is found to reduce variations in the wavefront by ~92%. Our result demonstrates that a serious barrier to achieving diffraction-limited seeing over the whole sky has been removed.

On 27 March 1999 from UT 5:42 to UT 6:00, 130 frames of four stars in Aquila ($\alpha = 19\,\mathrm{h}\,29.1\,\mathrm{m}$, $\delta = +2^\circ\,39'$) were collected using the Rotator/Adapter acquisition probe optics[9] of the 3.6 m Telescopio Nazionale Galileo[10,11] (TNG).

These four stars lie in an unusual configuration very suitable for our purposes (Fig. 1a). Three stars, ranging from $V \approx 9$ to $V \approx 11$, are arranged at the vertices of a nearly equilateral triangle with a fourth $V \approx 12$ star in its centre. The average distance of the three surrounding stars from the central one is about 15.4 arcsec (ref. 12). The frames have been collected with 0.1 seconds of exposure time on a Peltier-cooled CCD (charge-coupled device; ref. 13), deliberately introducing enough defocus to obtain an extra-focal pupil image for each star approximately 6 arcsec in diameter (Fig. 1b). Seeing was estimated to be 1.2 arcsec at the time of exposures. The central wavelength of observations was 700 nm. Since the delay between two subsequent exposures was of the order of 8 seconds, it is reasonable to assume that the turbulence distorting each image becomes totally uncorrelated after such a delay. During the 18 minutes needed to collect the whole set of frames, no evidence of a significant seeing variation was recorded. Data were collected after a whole night of observations during which thermalization between the telescope and the external environment was ensured. Elevation of the target was roughly 45°.

Those data were used to retrieve wavefront maps for each of the four stars and for any collected image (Fig. 1c). Wavefront maps show the amount of distortion in the optical path for any position in the pupil of the telescope. Instead of carrying out further calculations using the wavefront map as a whole, it is useful to express the latter as a linear combination of a defined set of functions. A suitable set is represented by Zernike polynomials[14]. The first ones convey a mathematical description of common Seidel aberrations (such as defocus, coma and astigmatism). These polynomials are conventionally ordered such that the higher their order, the weaker their statistical weight. Thus, for practical purposes, a wavefront map is described by a finite, sufficiently large, number of Zernike polynomials. We fitted each wavefront data with p classical Zernike polynomials up to a complete radial degree order (for instance $p = 27$ polynomials up to 6th radial degree, because the first term, that is the piston, is missing).

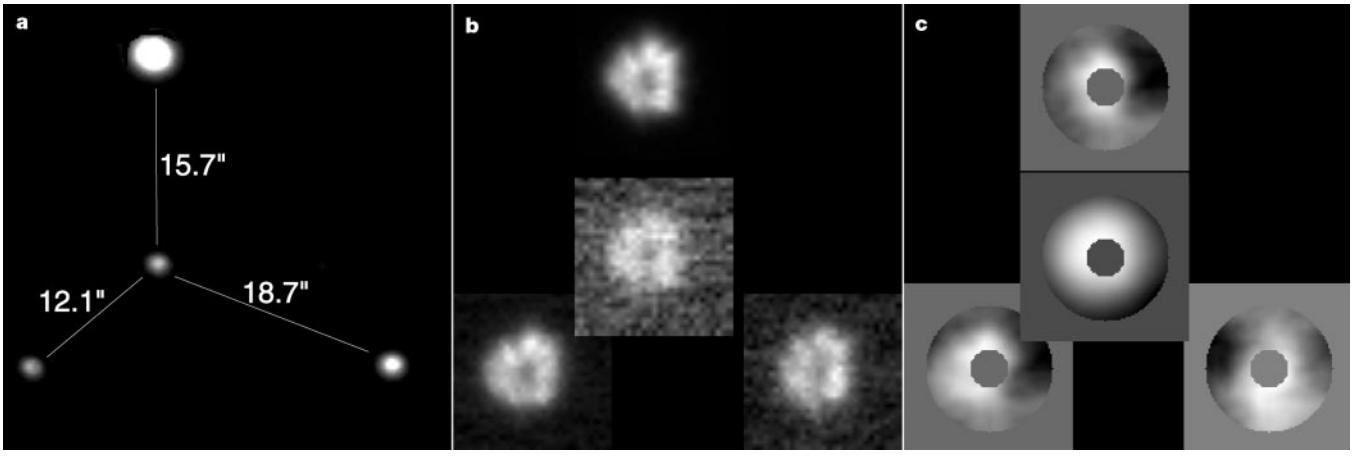

Figure 1 The four observed stars, an example of raw data and the corresponding wavefront maps. **a**, The four observed reference stars. The frames of the four defocused stars have been nominally corrected for detector sensitivity inhomogeneities. **b**, The four pupils have been extracted and stored in four data-cubes of 32 × 32 × 130 pixels each. **c**, Any single-pupil image has been used to retrieve wavefront maps[21,22], making use of a Fourier approach[23] to solve the Poisson equation. The wavefront of the central star and the differences between it and the other three are displayed. The starlight-brightness distribution on a defocused pupil depends on both the incoming wavefront curvature and the scintillation. The latter contribution may be cancelled out if, as usual, two extrafocal images are employed to retrieve the wavefront phase. Hickson[21] suggested using only one defocused pupil to reconstruct the wavefront shape, thus giving also an experimental demonstration of the technique feasibility[22]. Nevertheless, those results are still affected by scintillation, which is proportional to the wavefront curvature of each perturbing layer, weighted by its distance from the telescope pupil. In fact, as suggested by Ribak[24], such dependence can be used to disentangle, to a limited extent, the origin of the wavefront deformation. The final brightness distribution on the single defocused pupil is given by a linear combination of the wavefront perturbation contributions for each single layer. The conclusions reported here may be applied to all four reference stars, since the effect acts in the same manner. It is also worth noting that the scintillation effects slightly enhance the reliability of our measurements, because of a larger weighting on the high-altitude layers, which are most responsible for the decorrelation among the four reference stars.

It is reasonable that the integration time used (the minimum allowed by our camera) is significantly larger than the atmospheric turbulence correlation time. It means that only the features of a size larger than a characteristic length scale (given by the product of the exposure time and the wind speed) are retained, while the smaller size ones are attenuated. Thus, fitting the measured data with high-order Zernike polynomials is useless for our purposes. During our observing run, ground wind speed was 3 m s^{-1}, leading to a minimum length scale of ~0.3 m. Lacking precise wind-speed measurements at high altitudes, we chose to limit the fitted Zernike polynomials to the first 27.

Each star wavefront map is the result of the bidimensional projection along its direction of all the starlight deformations occurring on several layers at different altitudes. In principle, by combining the information from different stars the three-dimensional distribution of such turbulence can be retrieved. Thus, the turbulence bidimensional projection and the corresponding wavefront along any given line of sight can be estimated, regardless of the existence of a suitable reference star (Fig. 2). Expanding the various wavefront measurements in terms of Zernike polynomials, such an estimate can be described in a linear and compact form[8] by a modal tomographic matrix M.

Let us call W_T the Zernike polynomial expansion of the beam in the direction of the object of interest, represented by the fourth star at the centre of the quasi-equilateral triangle. Let $\mathbf{L}$ be the $3p$-dimensional vector of the p Zernike polynomial coefficients L_i, $1 \leqslant i \leqslant 3$, for each ith star at each vertex of the triangle. Modal tomography assumes the validity of the following relation:

$$W_T = M \cdot \mathbf{L} = M \cdot \begin{bmatrix} L_1 \\ L_2 \\ L_3 \end{bmatrix} \quad (1)$$

Matrix M has been computed row by row using the singular-value decomposition method. In the calculation we omit the piston term. In order to compute the best modal tomographic matrix M, we have maximized the achievable signal-to-noise ratio, using the whole data set.

The final results, displayed in Fig. 3, show that the subtraction of the average of the neighbouring stars (a slight enhancement to the conventional approach) reduces the variance of the single Zernike polynomials by a factor of 5.3 ± 3.3, while the best M found through the tomographic approach enables a variance reduction by a factor 16.8 ± 4.2. The large reduction of variance obtained with the simple average may be easily explained as consequence of a significant ground layer.

This experiment proves the feasibility of wavefront sensing in any given direction in the sky, using few off-axis reference stars. The latter can be at a distance much larger than the isoplanatic patch size, whose tiny dimension prevented the use of adaptive optics for whole-sky purposes.

The modal tomography matrix M depends upon the number, altitude and relative strength of the perturbing layers. All these parameters evolve with time and may significantly change during a single observation night. Hence the best matrix M, that is the one producing the best possible tomographic estimate, varies with time. The typical lifetime of M and the time interval to be used for its best estimation are new problems which need to be carefully addressed for the realization of tomographic adaptive optics systems. Even if restriction to a data subset could have led to the investigation of these interesting properties, in our case the augmented noise resulting from the averaging of a smaller number of independent measurements have hidden such effects.

Atmospheric turbulence distribution in altitude h is encoded in a function, usually denoted by $C_N^2(h)$, describing the importance of the air refractive-index fluctuations, causing starlight distortion. Although $C_N^2(h)$ should be treated as a continuous function, current views on turbulence arrangement suggest that $C_N^2(h)$ support is restricted to a finite, tiny number of limited regions around specific altitudes. It has been shown on general grounds[8] that M can be computed from the geometry of the star positions and knowledge of $C_N^2(h)$. An independent measure of such a function has not been carried out during our observation. This quantity could have permitted a comparison between the theoretical value of M and the actual one, obtained as a best estimate from our direct measurements. Nevertheless, our work proves the existence of an effective (in the sense of significant reduction of starlight aberration) matrix M, regardless of its similarity to the theoretical expected one.

Site characterization can thus be seen from a completely new point of view. A site characterized by a limited number of different perturbing layers, for which M is expected to be more effective and stable than in other cases, should be classified, to a certain extent, as a better site, regardless of the characteristics of turbulence seen projected over a single line of sight.

The tomographic approach we tested on natural stars may be applied to artificial references as well; these stars, obtained by the excitation of the natural mesospheric sodium layer through a powerful laser[15], immediately extend whole-sky diffraction-limited capability to telescopes of any size. However, a single artificial star cannot solely be used to close an adaptive optics loop. Such an artificial reference, in fact, forms at a limited altitude of ~90 km and the sampled atmosphere has a conical rather than cylindrical shape, leading to a wavefront estimation error known as conical anisoplanatism. This error scales with the telescope diameter and the

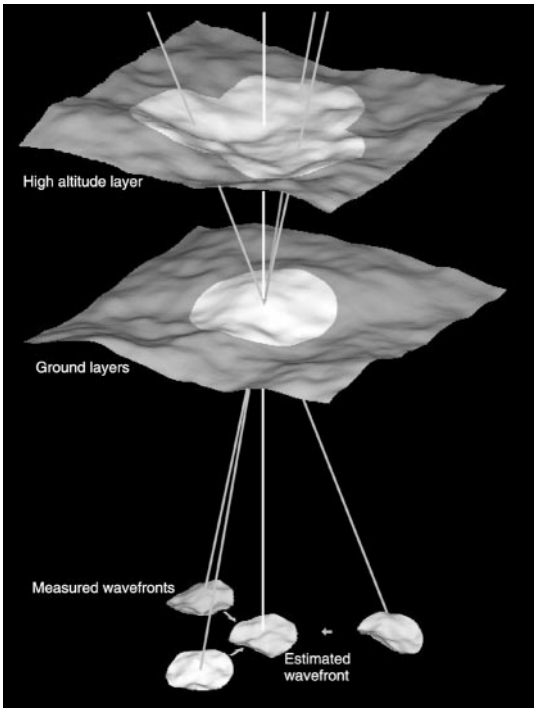

Figure 2 Tomographic measurement of starlight wavefronts exploits turbulence distribution in three dimensions. Light from the source is perturbed by different layers of the Earth's atmosphere. Here we examine two different layers (one is located very close to the ground, as usually happens). For instance, by observing three stars situated at a certain distance from the line of sight of the telescope (the three grey lines), three different starlight wavefront deformations are obtained. None of them can be used to correct on-axis distortion. Tomographic reconstruction of perturbation split into the layers allows us to estimate the wavefront perturbation for a direction (white line) where no reference star is present.

observing wavelength so that laser-guide-star adaptive-optics systems become unusable for 8-m-class telescopes observing in the visible band. Therefore, in order to overcome this problem, multiple laser-guide-stars should be arranged in a constellation.

Scaling up to larger telescope entrance pupils, the limits on the distance of reference stars to the line of sight, in the tomographic approach, are relaxed even further. Next generation 100-m-class telescopes[16,17] can reach extremely high performance ($V = 38$ with 10 h exposure time, for instance) on condition that they achieve diffraction-limited capabilities. Such a result can be obtained on the whole sky without the need of any artificial bright reference, thus preventing any spurious light pollution[18]. Combining this concept with recent ones[19], a limiting magnitude as faint as $V \approx 17$ should be found for a few stars in a patch of several tens of arcmin, in order to provide full turbulence compensation in such an area.

The next big technical challenge is the realization of an adaptive-optics system capable of effectively correcting, in real time, the wavefront approaching from a region of the sky free from bright references. The related concept of multi-conjugate adaptive optics[20] is well understood and our measurements, which are essentially open-loop ones, provide convincing proof that this class of systems, which inherently solve the tomographic problem in a closed-loop fashion, are effective. The efficiency and stability in closed-loop operations are usually much higher than in the open-loop case and, in our opinion, much better results are to be expected than any obtainable from open-loop measurements. Moreover, the technical problems posed by a tomographic approach open up new challenges for wavefront sensing: multiple objects need to be sensed with the aim of possibly detecting wavefront perturbations arising from layers located at different distances from the observer. This is a different problem with respect to the usual wavefront-sensing task in conventional adaptive optics. We think that very soon new classes of wavefront sensors will be realized and tested on the sky.

Such wavefront sensors will be both capable of adapting to the closed-loop situation and compatible with multiple-object wavefront sensing, and may be of use with 8-m-class telescopes leading to whole-sky, diffraction-limited capability, using solely natural stars. □

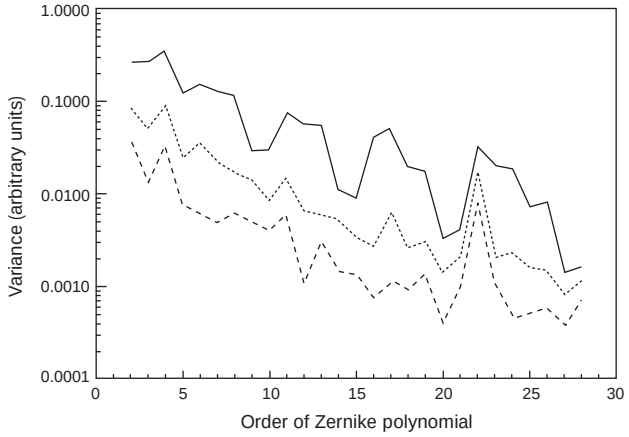

Figure 3 Atmospheric, conventional-technique-corrected and tomographic-corrected turbulence variances. The solid line shows each Zernike polynomial variance as measured on the central star, thus indicating the uncorrected turbulence starlight distortion that prevents diffraction-limited imaging with astronomical telescopes. We computed the residual polynomial variance obtained by subtracting from the central star the simple average of the surrounding ones (dotted line). This represents a somewhat trivial approach to the tomographic problem (actually, in this way no serious attempt at resolution is achieved), although in the special configuration observed, the hope of cancelling out the anti-correlated behaviour of high-altitude effects on the optical beams may be justifiable. This method allowed a 77.4% reductions of wavefront variance compared to that of central star. We compare this result with the average variance reduction determined by the subtraction of Zernike polynomials from each of the three surrounding stars. That procedure allows an average variance reduction of 71.2%. This slightly worse result may be interpreted as further evidence that measurements that are able to rule out the highest-altitude-layer contribution allow a partial correction based on a larger equivalent isoplanatic sky patch size. Such an outcome is in agreement with theoretical suggestions[25] and experimental evidence from Rayleigh-based laser guide star data[26]. The result shown in the plot is hence the best obtainable from conventional adaptive optics when a bright nearby star is not very close to the observed target. The dashed line indicates the residual polynomial variance computed by subtracting from the central star measurements the neighbouring star data, processed through model tomography matrix *M*. Note that the modal tomography concept allows an additional substantial improvement, reducing the uncorrected wavefront variance by 92.3%. In contrast to the previous case, there seems to be no evident theoretical limit to extending this technique in order to cancel out almost all starlight perturbation.

Received 18 May; accepted 15 October 1999.

1. Beckers, J. M. Adaptive optics for astronomy—principles, performance, and applications. *Annu. Rev. Astron. Astrophys.* **31,** 13–62 (1993).
2. Giacconi, R. *et al.* Science verification of the Unit Telescope 1 of the ESP Very Large Telescope. *Astron. Astrophys.* **343,** L1–L4 (1999).
3. Mountain, C. M., Gillet, F. C. & Oschmann, J. M. Gemini 8-m telescopes. *Proc. SPIE* **3352,** 2–13 (1998).
4. Tyson, R. K. *Principles of Adaptive Optics* (Academic, San Diego, 1991).
5. Roddier, F. Maximum gain and efficiency of adaptive optics systems. *Publ. Astron. Soc. Pacif.* **110,** 837–840 (1998).
6. Murphy, D. V., Primmermann, C. A., Zollars, B. G. & Barclay, H. T. Experimental demonstration of atmospheric compensation using multiple synthetic beacon. *Opt. Lett.* **16,** 1797–1799 (1991).
7. Tallon, M. & Foy, R. Adaptive telescope with laser probe—Isoplanatism and cone effect. *Astron. Astrophys.* **235,** 549–557 (1990).
8. Ragazzoni, R., Marchetti, E. & Rigaut, F. Modal tomography for adaptive optics. *Astron. Astrophys.* **342,** L53–L56 (1999).
9. Ragazzoni, R. Optics for the TNG Rotator/Adapter. *Telescopio Nazionale Galileo Tech. Rep.* **39** 1–8 (1994).
10. Barbieri, C. The Galileo Italian National telescope and its instrumentation. *Proc. SPIE* **2871,** 244–255 (1997).
11. Bortoletto, F. *et al.* Commissioning the Italian National Telescope Galileo. *Proc. SPIE* **3352,** 91–101 (1998).
12. Sinnott, R. W. Hunting for equilateral triple stars. *Sky Telesc.* March, 100–101 (1999).
13. Bortoletto, F. *et al.* CCD cameras for the Italian national telescope Galileo. *Proc. SPIE* **2654,** 248–258 (1996).
14. Noll, R. J. Zernike polynomials and atmospheric turbulence. *J. Opt. Soc. Am.* **66,** 207–211 (1976).
15. Happer, W., MacDonald, G. J., Max, C. E. & Dyson, F. J. Atmospheric-turbulence compensation by resonant optical backscattering from the sodium layer in the upper atmosphere. *J. Opt. Soc. Am.* **11-A,** 263–276 (1994).
16. Gilmozzi, R. *et al.* Future of filled aperture telescopes: is a 100-m feasible? *Proc. SPIE* **3352,** 778–791 (1998).
17. Mountain, C. M. What is beyond the current generation of groundbased 8-m to 10-m class telescopes and the VLT-I? *Proc. SPIE* **2871,** 579–606 (1997).
18. Ragazzoni, R. No laser guide stars for adaptive optics in giant telescopes? *Astron. Astrophys. (Suppl.)* **136,** 205–209 (1999).
19. Ragazzoni, R. & Farinato, J. Sensitivity of a pyramidic wave front sensor in closed loop adaptive optics. *Astron. Astrophys.* **350,** L23–L26 (1999).
20. Beckers, J. M. Detailed compensation of atmospheric seeing using multiconjugate adaptive optics. *Proc. SPIE* **114,** 215–217 (1989).
21. Hickson, P. Wave-front curvature sensing from a single defocused image. *J. Opt. Soc. Am. A* **11,** 1667–1673 (1994).
22. Hickson, P. Single-image wavefront curvature sensing. *Proc. SPIE* **2201,** 549–554 (1994).
23. Roddier, F. & Roddier, C. Wavefront reconstruction using iterative Fourier transforms. *Appl. Opt.* **30,** 1325–1327 (1991).
24. Ribak, E. N. Atmospheric scintillations for measuring remote wave fronts. *Proc. SPIE* **2580,** 166–172 (1995).
25. Ragazzoni, R. & Marchetti, E. Rayleigh vs. Sodium beacon for large FoV partial correction. *Atmos. Ocean. Opt.* **8,** 174–176 (1995).
26. Christou, J. C., Ellerbroek, B., Fugate, R. Q., Bonaccini, D. & Stanga, R. Rayleigh beacon adaptive optics imaging of ADS 9731: Measurements of the isoplanatic field of view. *Astrophys. J.* **450,** 369–379 (1995).

Acknowledgements

We thank the Telescopio Nazionale Galileo commissioning team, led by F. Bortoletto, including C. Bonoli, A. Cavazza, L. Corcione, M. D'Alessandro, D. Fantinel, D. Gardiol, A. Ghedina, E. Giro, J. C. Guerra Ramón, D. Mancini, J. L. Medina, F. Paulli, C. Pernechele, P. Schipani, G. Tessicini, G. Trancho Lemes, C. Vuerli and A. Zacchei for their invaluable work. Special thanks are also due to L. Salvadori.

Correspondence and requests for materials should be addressed to R.R. (e-mail: ragazzoni@pd.astro.it).